Anderson Localization of Composite Excitations in Disordered Optomechanical Arrays

Thales Figueiredo Roque,[1] Vittorio Peano,[2] Oleg M. Yevtushenko,[2] and Florian Marquardt[2,3]

[1] *Instituto de Física Gleb Wataghin, Universidade Estadual de Campinas, 13083-859 Campinas, São Paulo, Brazil*
[2] *Institute for Theoretical Physics II, University Erlangen-Nürnberg, D-91058 Erlangen, Germany*
[3] *Max Planck Institute for the Science of Light, Günther-Scharowsky-Straße 1, D-91058 Erlangen, Germany*

(Dated: July 15, 2016)

Optomechanical arrays are a promising future platform for studies of transport, many-body dynamics, quantum control and topological effects in systems of coupled photon and phonon modes. We introduce disordered optomechanical arrays, focusing on features of Anderson localization of hybrid photon-phonon excitations. It turns out that these represent a unique disordered system, where basic parameters can be easily controlled by varying the frequency and the amplitude of an external laser field. We show that the two-species setting leads to a non-trivial frequency dependence of the localization length for intermediate laser intensities. This could serve as a convincing evidence of localization in a non-equilibrium dissipative situation.

PACS numbers: 42.50.Wk, 71.55.Jv, 42.65.Sf

arXiv:1607.04159v1 [cond-mat.mes-hall] 14 Jul 2016

Introduction: Optomechanics is a rapidly evolving research field at the intersection of condensed matter and quantum optics [1, 2]. By exploiting radiation forces, light can be coupled to the mechanical motion of vibration modes. The interplay of light and motion is now being used for a range of applications, from sensitive measurements to quantum communication, while it also turns out to be of significant interest for fundamental studies of quantum physics.

This rapidly developing area has so far mostly exploited the interaction between a single optical mode and a single mechanical mode. Going beyond this, recent theoretical research indicates the substantial promise of so-called optomechanical arrays, where many modes are arranged in a periodic fashion. In such systems, a large variety of new phenomena and applications is predicted to become accessible in the future. These include the quantum many-body dynamics of photons and phonons [3], classical synchronization and nonlinear pattern formation [4–6], tunable long-range coupling of phonon modes [7–9], photon-phonon polariton bandstructures and transport [10, 11], artificial magnetic fields for photons [12], and topological transport of sound and light [13]. A first experimental realization of a larger-scale optomechanical array has recently been presented, involving seven coupled optical microdisks [14]. Even greater potential is expected for implementations based on optomechanical crystals [15–17], i.e photonic crystals that can be patterned specifically to generate localized photon and phonon modes.

Given these promising predictions and the rapid experimental progress towards larger arrays, the question of disorder effects now becomes of urgent importance. For example, in the case of optomechanical crystals, experiments indicate fluctuations in the geometry of about 1%, which translate into equally large relative fluctuations of both the mechanical and optical resonance frequencies. This will invariably have a very significant impact on the transport properties. However, gaining a better understanding of disorder effects in the various envisaged applications is only one motivation of the research to be presented here. Of equal, possibly even greater, importance is the opportunity that is offered by optomechanics to create a highly tuneable novel platform for deliberately studying fundamental physical concepts such as Anderson localization [18].

Localization of waves in a random potential is one of the most remarkable and nontrivial interference effects. Initially, it has been studied in electronic disordered systems [19], though this effect applies equally to other types of quantum and even classical waves [20]. By now, localization and related phenomena have been discovered and investigated in photonic systems [21–27], coupled resonator optical waveguides [28], cold atomic gases [29, 30], in propagation of acoustic waves [31] and in Josephson junction chains [32]. Localization can even play a constructive role, namely in random lasing [27, 33]. In spite of extensive theoretical efforts, the unambiguous interpretation of experimental manifestations of localization often remains a challenge, even in situations where the ideal version of Anderson localization applies.

Optomechanical arrays enable controlled optical excitation and readout and at the same time promise significant flexibility in their design. However, it is the optical tuneability of the interaction between two different species (photons and phonons) that makes optomechanical systems a unique platform. As we will show in the present Letter, this offers an opportunity to study effects in Anderson localization physics which currently represent a significant challenge even on the theoretical level and will thus open the door towards exploring novel physics that has not been observed so far.

The model: We consider a 1D array of optomechanical cells (OMA), see Fig.1, driven by a single bright laser. The cell j contains an optical and a vibrational mode that are coupled via the standard linearized optomechanical

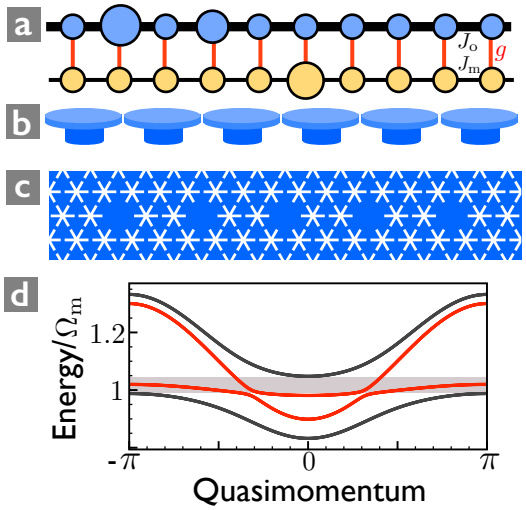

FIG. 1. (color on-line) Scheme, implementations and band structure of an optomechanical array. (a) An array of photon (blue dots) and phonon (yellow) modes can be viewed as a ladder: photons and phonons either can hop to nearest neighbor sites or can be interconverted on the same site. This system can be implemented by (b) an array of microdisks, or (c) an array of co-localized optical and mechanical defect modes in an optomechanical crystal. (d) Optomechanical band structure for two different values of the coupling $g/\Omega_m = 0.01, 0.1$ (red/black lines). For the larger interaction strength the upper and lower polariton bands are separated by a complete band gap (grey region). The other parameters are $\Omega_o = 1.1\Omega_m, J_o = 0.1\Omega_m, J_m = 0.01\Omega_m$.

Hamiltonian

$$\hat{H}_j = \sum_{\nu=o,m} \omega_{\nu,j}\, \hat{n}_{\nu,j} - g_j \left(\hat{c}_{o,j} + \hat{c}^\dagger_{o,j}\right)\left(\hat{c}_{m,j} + \hat{c}^\dagger_{m,j}\right); \quad (1)$$

see Refs.[1, 34] for details. Here $\hat{n}_{\nu,j} \equiv \hat{c}^\dagger_{\nu,j}\hat{c}_{\nu,j}$, and $\hat{c}_{\nu,j}$ is the bosonic annihilation operator of either optical, $\nu =$ "o", or mechanical, $\nu =$ "m", excitations (we set $\hbar = 1$). Due to disorder, the frequencies $\omega_{\nu,j}$ fluctuate around mean values $\langle\omega_{\nu,j}\rangle_d = \Omega_\nu$. We assume that $\omega_{\nu,j}$ are independent Gaussian random variables with variances $\langle(\omega_{\nu,j} - \Omega_\nu)(\omega_{\nu',j'} - \Omega_{\nu'})\rangle_d = \sigma^2_\nu \delta_{j,j'}\delta_{\nu,\nu'}$. Eq. (1) is defined in a rotating frame, where the optical frequencies $\omega_{o,j}$ are counted off from the laser frequency, ω_L [1]. Thus, Ω_o indicates the average detuning and can be tuned in situ by varying the laser frequency. The optomechanical couplings g_j are proportional to the mean amplitude of the light circulating in the cavity j [1]. Hence, they are also tunable by varying the laser power.

The presence of two-mode squeezing interactions in Eq. (1) can in principle lead to instabilities. We choose Ω_o such that these terms are off-resonant and disorder configurations with optical [35] or vibrational instabilities are very rare. We leave their study for a forthcoming paper.

We can describe the full OMA by a Hamiltonian with nearest-neighbor optical, J_o, and mechanical, J_m, hopping amplitudes:

$$\hat{H} = \sum_j \hat{H}_j - \hat{H}_{\rm h}, \quad \hat{H}_{\rm h} = \sum_{j,\nu} J_\nu \hat{c}^\dagger_{\nu,j+1}\hat{c}_{\nu,j} + H.c. \quad (2)$$

Our model is time-reversal symmetric [36].

Clean polariton bands: In a clean OMA without dissipation (and without squeezing interaction), the photon–phonon hybridization leads to a pair of bands with energies

$$\Omega_\pm = \bar{\Omega} - 2\bar{J}\cos(k) \pm \sqrt{[\delta\Omega/2 - \delta J\, \cos(k)]^2 + g^2}, \quad (3)$$

where $\bar{\Omega} = (\Omega_o + \Omega_m)/2$, $\delta\Omega = (\Omega_o - \Omega_m)$ and likewise for $\bar{J}$, δJ. We refer to $\Omega_\pm$ as upper/lower polariton band, respectively. k denotes the wave-vector of polaritonic Bloch states. We focus on the regime where the uncoupled bands overlap, $\delta\Omega < 4\bar{J}$. In this case, the polariton bands are separated by a gap if the coupling becomes large enough, $g > g_{\rm min}$ [37], see Fig.1.

Anderson localization of uncoupled excitations: It is well known that even weak disorder leads to a crucial effect in a 1D system: the eigenstates become localized. If $g = 0$, each subsystem (photon/phonon), is individually described by the 1D Anderson model [18]. The localized states decay exponentially away from their center, $\sim \exp(-|j - j_0|/\xi^{(0)}_\nu)$. Here $\xi^{(0)}_{o,m}$ are the bare localization lengths for photons and phonons (for $g = 0$), measured in units of the lattice constant. Using the theory of 1D localization [38], we can approximate the frequency dependence of the localization length:

$$\xi^{(0)}_\nu(\Omega) \simeq 2(2\sin[k_\nu(\Omega)]/\chi_\nu)^2; \quad (4)$$

here the dimensionless quantities $\chi_\nu \equiv \sigma_\nu/J_\nu$ and $2\sin[k_\nu]$ are the disorder strength and the bare group velocity, respectively. Eq.(4) is valid for weak (up to moderately strong) disorder [39]. The comparison of Eq.(4) with numerical results is shown below in Fig.3.

In any experiment, localization can be detected if photons and phonons explore the localization length before leaking out, at a rate $\kappa_{o,m}$. This holds true if $\xi_\nu < 2J_\nu|\sin(k_\nu)|/\kappa_\nu$, which allows us to neglect dissipation in a first approximation [40]. In addition, the sample size L should be larger than the localization length, $L \gg \max(\xi^{(0)}_\nu)$. For typical $L \sim 100$ we need $\max(\xi^{(0)}_\nu) \sim 10$, corresponding to $\chi_\nu \sim 1$.

Localization in Optomechanical Arrays: At finite photon-phonon coupling, we encounter an Anderson model with two channels. Localization in the symmetric version of this model (with equal parameters of each channel) is well studied and understood [41, 42]. However, OMAs do not fall into this universality class since the mechanical band is generically much narrower than the optical

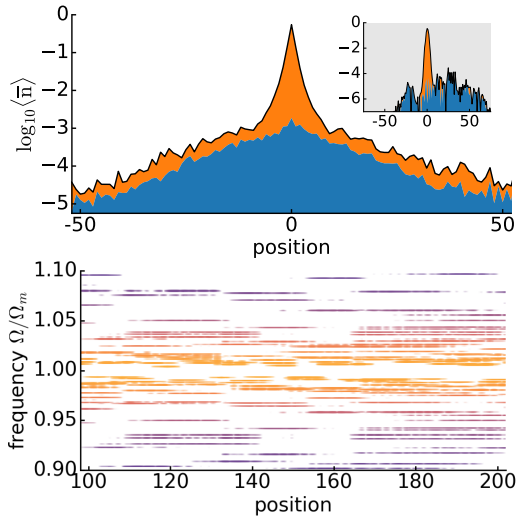

FIG. 2. (color on-line) Upper panel: Typical shape of an eigenstate, at $\Omega_o = \Omega_m$, $g = 0.001\Omega_m$, without disorder averaging (inset) and after disorder averaging over 500 realizations (main picture). Other parameters are explained in the text. Two different localization lengths are clearly visible. The profiles of $\bar{n}_j$, obtained from different disorder realizations, have been shifted in space, such that their maxima are always located at $j = 0$. Lower panel: Local density of states (frequency- and position-resolved spectrum) at $g = 0.05\Omega_m$; other parameters as in the upper panel. The color ranges from orange to blue, depending on whether a given eigenstate has a stronger mechanical or optical component, respectively.

one, $J_m \ll J_o$. Thus, the hybrid excitations consist of two components with very different velocities. Similar composite quasiparticles are not uncommon, another example is given by cavity polaritons [43, 44] including polaritons in a disordered potential [45]. Developing the theory of localization for such non-symmetric systems remains a real challenge, cf. Ref.[46]. The hybrid localized states typically have two localization lengths, $\xi_1 < \xi_2$, see the upper panel of Fig.2. For small systems, $L < \xi_1$, the excitations do not feel localization and propagate ballistically. Their transmission decays as $\exp(-L/\xi_1)$ in the range $\xi_1 < L < \xi_2$ and becomes suppressed as $\exp(-L/\xi_2)$ at $L > \xi_2$. Our numerical analysis shows that the space region where ξ_1 dominates quickly shrinks with increasing g. Therefore, ξ_2 seems more interesting experimentally, and we will focus on this 'large' localization length in the following. We start from a numerical analysis for relatively strong disorder. At the first stage, we neglect disorder-induced fluctuations of g_j [47] and use its homogeneous mean value $g = \text{const}$.

The method: The localization length can be obtained, e.g., from the photon-photon transmission, $T_{oo}(j,k;\Omega) \propto \left|G^R_{oo}(j,k;\Omega)\right|^2$ where $G^R_{oo}(j,k;\Omega) = -i\int_0^\infty dt \exp(i\Omega t)[\hat{c}_{o,j}(t), \hat{c}^\dagger_{o,k}(0)]$ is the frequency-resolved retarded Green's function. T_{oo} is defined via the optical power detected on site j at frequency $\omega_L + \Omega$ while a probe laser of the same frequency is impinging on a different site k [48]. For $x = |j-k| \to \infty$, we expect $T_{oo}(j,k;\Omega) \propto \exp(-2x/\xi_2)$. Thus, the expression for the averaged (inverse) localization length reads

$$\xi_2^{-1}(\Omega) = -\lim_{x\to\infty}\left(\left\langle \ln\big(T_{oo}(j,k;\Omega)\big)\right\rangle_d \Big/ 2x\right). \quad (5)$$

We note that the value of $\xi_2(\Omega)$ is the same for other transmission processes (e.g. photon-phonon transmission) [48].

Eq.(5) can be used as a definition even in the presence of dissipation. In the absence of dissipation and instabilities, there is a simpler alternative, namely extracting the localization length directly from the spatial profile of eigenstates [48]. To ensure reliability of results, we have combined both approaches in numerical simulations.

Analysis of numerical results: The upper panel of Fig.2 shows a typical optomechanical eigenstate in the case of small coupling. The excitation frequency has been selected from the tail of the pure mechanical band. Two different slopes, which correspond to two different localization lengths $\xi_{1,2}$, are clearly visible. When g increases and the other parameters of the upper Fig.2 remain unchanged, the region where ξ_1 dominates shrinks [49] and becomes invisible very quickly. In the following, we will concentrate on ξ_2 and will denote it as ξ for the sake of brevity. The lower panel of Fig.2 illustrates the distribution of optomechanical excitations in space and frequency, including the character of excitations (photon vs. phonon).

Here, and in the following, we have displayed numerical results for an illustrative set of parameters: $J_o = 0.1\Omega_m \gg J_m = 10^{-3}\Omega_m$. Localization of the optomechanical excitations becomes pronounced at $\chi_{o,m} \sim 1$. For concreteness, we have chosen equal relative disorder strength, $\chi_o = \chi_m = 1$. In real samples, J_o ranges from 1GHz to 10THz (J_m: from 100kHz to 1GHz) with the optical disorder being of order 100GHz to 1THz (mechanical: from 10MHz to 100MHz). Thus, our choice of $\chi_{o,m}$ falls into the range of experimentally relevant parameters. The optomechanical coupling in our numerics ranges from weak, $g = 10^{-3}\Omega_m$, to strong, $g = 0.05\Omega_m$. To suppress finite size effects, we employed large systems, $L = 10^3 \gg \xi$, during exact diagonalization. The Green's functions method has allowed us to explore even much larger sizes.

In Fig.3, we display the frequency-dependence of the localization length of hybrid optomechanical excitations in a disordered array, one of the central numerical results of this article. For comparison, we also show the situation for the uncoupled systems, including the (scaled) analytical expression for $\xi_o^{(0)}$, Eq.(4) [50] (green solid line in Fig.3a). Once the subsystems are coupled, significant changes of $\xi(\Omega)$ occur in the vicinity of the unperturbed (narrow) mechanical band where the optomechanical hybridization is most efficient. Firstly we note that, if

$0 < g < \Delta^{(m)}_{\rm loc}$, the coupling between the optical and the mechanical systems is perturbatively weak even in the middle of the mechanical band [region I in Fig.3(f)]. On the other hand, when the optomechanical coupling becomes large, $g > \sqrt{J_o J_m} = \sqrt{\sigma_o \sigma_m} \sim \Delta^{(o)}_{\rm loc}$ for our choice of parameters, a gap opens around the resonant frequency $\Omega = \Omega_m$ and remaining excitations inside the gap tend to become localized [Fig.3(e)].

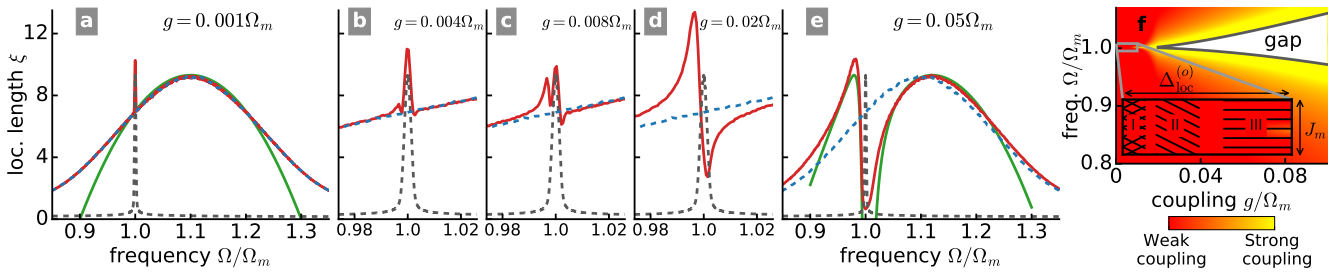

FIG. 3. (color on-line) Frequency-dependence of the localization length: Dashed lines show bare ($g = 0$) optical ($\xi^{(0)}_o$ - blue) and mechanical ($\xi^{(0)}_m$ - black) localization lengths. The red solid line shows the localization length of hybrid excitations, ξ, calculated at several values of the optomechanical coupling, $0.001\Omega_m \le g \le 0.05\Omega_m$, and $\Omega_o = 1.1\Omega_m$. Green solid lines describing $\xi^{(0)}_o$ in panel (a) and ξ in panel (e) are obtained from Eqs.(4,6), respectively, after scaling by a constant factor. Panel (f) illustrates schematically the different regimes as a function of coupling and frequency.

Analytical methods which would allow one to explore localization in strongly disordered systems are not available in general. Nevertheless, it turns out that our optomechanical array corresponds to a certain two-channel system, which was studied analytically in Ref.[46] for the limit of weak disorder and large coupling. Remarkably, the shape of our numerically extracted $\xi(\Omega)$ at large g agrees with the predictions of Ref.[46], even though we are here dealing with strong disorder, $\chi_\nu \sim 1$ [42]. The theory of Ref.[46] is valid if g is large compared with the (bare) mean level spacing in the localization volume, $\Delta^{(\nu)}_{\rm loc}$, which holds true for the parameters of our numerical study at $g \ge 0.05\Omega_m$ [51]. If $g > g_{\rm min}$, (i.e., if the clean polariton bands are separated by the gap of the width $\Omega_+(k=0) - \Omega_-(k=\pi)$) we can use the following (leading in χ_ν) expression for the localization length [46]:

$$\xi(\Omega) \simeq 4\big(2\sin\left[k_\pm(\Omega)\right]\big)^2 \big/ \big(\chi^2\left[1+\cos^2(\gamma)\right]\big)\,; \qquad (6)$$
$$\tan(\gamma) = 2\sqrt{J_o J_m}\, g/\delta J(\Omega - \Omega_r), \quad \Omega_r \equiv J_o \delta\Omega/\delta J.$$

Here $\chi = \chi_o/\mathcal{C} = \chi_m/\mathcal{C}$ and $k_\pm(\Omega)$ denotes the inverted dispersion relation $\Omega_\pm(k)$. The quantity $V_\pm \equiv 2\sin\left[k_\pm(\Omega)\right]$ is called "rapidity". It coincides with the group velocity of the excitations for $g = 0$, and according to Eq.(6) it governs the frequency-dependence of $\xi(\Omega)$ in the coupled case. The factor $\mathcal{C}$ reflects renormalization of the disorder strength caused by the optomechanical coupling. Calculation of $\mathcal{C}$ is beyond the scope of Ref.[46] and we have found its approximate value $\mathcal{C} \simeq 1.16$ by fitting the analytically calculated maximal value of $\xi(\Omega > \Omega_m)$ to the numerical one. Fig.3e shows the comparison of the analytical and numerical results. They differ noticeably only close to edges of the clean band where the analytical theory looses its validity because $\xi \to 1$. In addition, the gap is smeared by the relatively strong disorder.

We have discovered that, at $\Omega \simeq \Omega_m$, the crossover between small and large values of g is highly non-trivial (and it is outside the scope of the analytical theory): when the optomechanical coupling increases from $g \sim \Delta^{(m)}_{\rm loc}$ to $g \sim J_m$ [region II in Fig.3(f)], the single maximum of ξ [cf. Fig.3(a)→(b)] grows sublinearly in g [52]. This growth stops and turns into a decrease when $g \gg J_m$. Simultaneously, a new local maximum develops at the frequency corresponding to the maximum of the rapidity [Fig.3(b)→(c) and region III in Fig.3(f)]. Finally, the new local maximum becomes the global one and a dip appears close to Ω_m at $g \ge \Delta^{(o)}_{\rm loc}$ [Fig.3(c)→(d)]. This non-trivial dependence of the localization length on the coupling constant, i.e., on the tuneable intensity of the external laser, could help to distinguish localization and trivial dissipation effects in real experiments.

We have checked that the shape of $\xi(\Omega)$ is robust with respect to dissipation effects as long as the mean level spacing in the localization volume of the hybrid excitations is larger than the optical and mechanical decay rates, κ_ν [53]. Propagation of the excitations is suppressed due to their finite life time which is reflected by the frequency-independent decrease of ξ. Typical profiles $\xi(\Omega)$ are shown in Fig.4 where the optical dissipation rate increases until $\kappa_o = 0.1\Omega_m$. These profiles are also robust with respect to the spatial inhomogeneity of g_j which results from randomness of the cell frequencies [47, 54].

Conclusions and discussion: Disordered OMAs belong to a new class of disordered systems where composite (photon-phonon) excitations are localized and the most

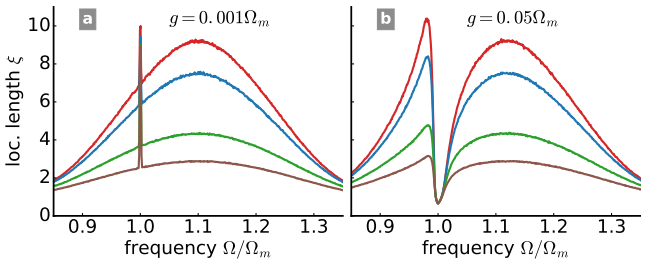

FIG. 4. (color on-line) Frequency-dependence of the localization length at $\Omega_o = 1.1\Omega_m$ and $g/\Omega_m = \{0.001, 0.05\}$ calculated for different values of the optical decay rate $\kappa_o/\Omega_m = \{0, 0.01, 0.05, 0.1\}$ (red-, blue-, green-, and brown lines, respectively). Note that the peak at $g = 0.001\Omega_m$ and $\Omega = \Omega_m$ is almost insensitive to the optical dissipation since the corresponding wavefunctions have mainly mechanical components.

important parameters can be easily fine-tuned. Thus, OMAs provide a unique opportunity to study Anderson localization of composite particles in real experiments. Moreover, they should allow to reliably distinguish localization from trivial dissipation effects. Future studies may address the additional novel physics that will arise when two-mode squeezing processes become relevant. At strong driving, this could involve the interplay between instabilities and localization, with interesting connections to random lasing, extending the new research domain of disordered optomechanical arrays into the nonlinear regime.

We acknowledge support from the EU Research Council through the grant EU-ERC OPTOMECH 278320. TFR acknowledges support from FAPESP. We are grateful to Vladimir Kravtsov and Igor Yurkevich for useful discussions.

[1] M. Aspelmeyer, T. Kippenberg, and F. Marquardt, Rev. Mod. Phys. **86**, 1391 (2014).
[2] M. Aspelmeyer, S. Groeblacher, K. Hammerer, and N. Kiesel, Journal of the Optical Society of America B **27**, A189 (2010).
[3] M. Ludwig and F. Marquardt, Phys. Rev. Lett. **111**, 073603 (2013).
[4] G. Heinrich, M. Ludwig, J. Qian, B. Kubala, and F. Marquardt, Phys. Rev. Lett. **107**, 043603 (2011).
[5] C. A. Holmes, C. P. Meaney, and G. J. Milburn, Phys. Rev. E **85**, 066203 (2012).
[6] R. Lauter, C. Brendel, S. J. M. Habraken, and F. Marquardt, Phys. Rev. E **92**, 012902 (2015).
[7] A. Xuereb, C. Genes, and A. Dantan, Phys. Rev. Lett. **109**, 223601 (2012).
[8] A. Xuereb, C. Genes, G. Pupillo, M. Paternostro, and A. Dantan, Phys. Rev. Lett. **112**, 133604 (2014).
[9] M. Schmidt, M. Ludwig, and F. Marquardt, New J. Phys. **14**, 125005 (2012).
[10] W. Chen and A. A. Clerk, Phys. Rev. A **89**, 033854 (2014).
[11] M. Schmidt, V. Peano, and F. Marquardt, New Journal of Physics **17**, 023025 (2015).
[12] M. Schmidt, S. Kessler, V. Peano, O. Painter, and F. Marquardt, Optica **2**, 635 (2015).
[13] V. Peano, C. Brendel, M. Schmidt, and F. Marquardt, Phys. Rev. X **5**, 031011 (2015).
[14] M. Zhang, S. Shah, J. Cardenas, and M. Lipson, Phys. Rev. Lett. **115**, 163902 (2015).
[15] A. H. Safavi-Naeini, T. P. M. Alegre, M. Winger, and O. Painter, Appl. Phys. Lett. **97**, 181106 (2010).
[16] J. Chan, A. H. Safavi-Naeini, J. T. Hill, S. Meenehan, and O. Painter, Applied Physics Letters **101**, 081115 (2012).
[17] A. H. Safavi-Naeini, J. T. Hill, S. Meenehan, J. Chan, S. Gröblacher, and O. Painter, Phys. Rev. Lett. **112**, 153603 (2014).
[18] P. W. Anderson, Phys. Rev. **109**, 1492 (1958).
[19] B. Kramer and A. MacKinnon, Reports on Progress in Physics **56**, 1469 (1993).
[20] M. C. W. van Rossum and T. M. Nieuwenhuizen, Rev. Mod. Phys. **71**, 313 (1999).
[21] A. A. Chabanov, M. Stoytchev, and A. Z. Genack, Nature **404**, 850 (2000).
[22] T. Schwartz, G. Bartal, S. Fishman, and M. Segev, Nature **446**, 52 (2007).
[23] S. Mookherjea, J. S. Park, S.-H. Yang, and P. R. Bandaru, Nature Photonics **2**, 90 (2008).
[24] Y. Lahini, A. Avidan, F. Pozzi, M. Sorel, R. Morandotti, D. N. Christodoulides, and Y. Silberberg, Phys. Rev. Lett. **100**, 013906 (2008).
[25] V. Savona, Phys. Rev. B **83**, 085301 (2011).
[26] M. Segev, Y. Silberberg, and D. N. Christodoulides, Nature Photonics **7**, 197 (2013).
[27] J. Liu, P. D. Garcia, S. Ek, N. Gregersen, T. Suhr, M. Schubert, J. Mørk, S. Stobbe, and P. Lodahl, Nature Nanotechnology **9**, 285 (2014).
[28] M. Hafezi, E. A. Demler, M. D. Lukin, and J. M. Taylor, Nature Physics **7**, 907912 (2011).
[29] J. Billy, V. Josse, Z. Zuo, A. Bernard, B. Hambrecht, P. Lugan, D. Clement, L. Sanchez-Palencia, P. Bouyer, and A. Aspect, Nature **453**, 891 (2008).
[30] G. Roati, C. D'Errico, L. Fallani, M. Fattori, C. Fort, M. Zaccanti, G. Modugno, M. Modugno, and M. Inguscio, Nature **453**, 895 (2008).
[31] H. F. Hu, A. Strybulevych, J. H. Page, S. E. Skipetrov, and B. A. van Tiggelen, Nature Physics **4**, 945 (2008).
[32] D. M. Basko and F. W. J. Hekking, Phys. Rev. B **88**, 094507 (2013).
[33] D. S. Wiersma, Nature **4**, 359 (2008).
[34] Derivation of the standard optomechanical Hamiltonian is briefly reviewed in Suppl.Mat.1.
[35] L. Mandel and E. Wolf, *Optical coherence and quantum optics* (Cambridge Univ. Press, Cambridge, 2008).
[36] This means that $J_{o,m}, g_0$ and g are real.
[37] The value of $g_{\min}$ is found from the condition $\Omega_+(k = 0) = \Omega_-(k = \pi) \Rightarrow g_{\min} = 2\mathrm{Re}\sqrt{J_o J_m \left(1 - [\delta\Omega/4\bar{J}]^2\right)}$.
[38] V. I. Melnikov, Sov. Phys. Solid State **23**, 444 (1981).
[39] Strictly speaking, one must require $\chi_\nu < 1$ though a softer condition $\xi_\nu \gg 1$ sufficies for practical purposes.
[40] We have taken into account that, in 1D systems, the excitations propagate ballistically in the localization volume.
[41] O. N. Dorokhov, Solid State Communications **44**, 915 (1982).

[42] P. A. Mello and N. Kumar, *Quantum transport in mesoscopic systems* (Oxford Univ. Press, Oxford, 2004).

[43] J. Kasprzak, M. Richard, S. Kundermann, A. Baas, P. Jeambrun, J. M. J. Keeling, F. M. Marchetti, M. H. Szymanska, R. Andre, J. L. Staehli, V. Savona, P. B. Littlewood, B. Deveaud, and L. S. Dang, Nature **443**, 409 (2006).

[44] E. Wertz, L. Ferrier, D. D. Solnyshkov, R. Johne, D. Sanvitto, A. Lemaitre, I. Sagnes, R. Grousson, A. V. Kavokin, P. Senellart, G. Malpuech, and J. Bloch, Nature Physics **6**, 860 (2010).

[45] F. Manni, K. G. Lagoudakis, B. Pietka, L. Fontanesi, M. Wouters, V. Savona, R. Andre, and B. Deveaud-Pledran, Phys. Rev. Lett. **106**, 176401 (2011).

[46] H.-Y. Xie, V. E. Kravtsov, and M. Müller, Phys. Rev. B **86**, 014205 (2012).

[47] g_j is proportional to the mean occupation number of the photons on the site j while the cells with smaller optical frequencies host more photons. This locally enchances g_j on these sites.

[48] Algebraic details for the derivation of the localization radius can be found in Suppl.Mat.2.

[49] If g increases and the other parameters of the upper Fig.2 remain unchanged, ξ_2 slightly increases. This might lead to suppression of the region where ξ_1 dominates because the eigenstate is normalized.

[50] The accuracy of Eq.(4) is insufficient to reproduce the maximal value of $\xi_o^{(0)}(\Omega_o)$ at the relatively strong optical disorder, $\chi_o = 1$. Therefore, we have scaled the analytical answer by a constant factor to adjust the heights.

[51] The mean level spacing in the localization volume is obtained from the relation $\Delta_{\rm loc}/\Delta = N/\xi$. Using the estimate for the mean level spacing in a band of extremely localized states $\Delta \sim \delta/N$ [55, 56], we find $\Delta_{\rm loc}^{(\nu)} \sim \delta_\nu/\xi_\nu^{(0)} \sim J_\nu/\xi_\nu^{(0)}$. Here $\xi_\nu^{(0)}$ denotes bare (at $g = 0$) localization lengths. For the chosen parameters, this yields the condition $g > 10^{-1}\max\{J_\nu\} \sim 10^{-2}\Omega_m$. Thus, the analytical theory from Ref.[46] can be used to understand the case $g = 0.05\Omega_m$ while smaller values of g are beyond the validity range of the analytic expressions.

[52] The increase of $\xi_2(\Omega \simeq \Omega_m)$ when the optomechanical coupling is small, $g < J_m$, is explained in Suppl.Mat.3.

[53] Equivalently, we can require that the localization length is much smaller than the escape length.

[54] This robustness is exemplified in Suppl.Mat.4.

[55] O. Yevtushenko and V. E. Kravtsov, J. Phys. A **36**, 8265 (2003).

[56] O. Yevtushenko and V. E. Kravtsov, Phys. Rev. E **69**, 026104 (2004).

SUPPLEMENTAL MATERIALS

1. Standard optomechanical Hamiltonian

The linearized Hamiltonian, Eq.(2) of the main text, is derived starting from the Hamiltonians of a phononic and a photonic array. In the tight-binding approximation, both Hamiltonians take the same form,

$$\hat{H}_\nu = \sum_j \left\{ \omega_{\nu,j}\, \hat{c}^\dagger_{\nu,j}\hat{c}_{\nu,j} - J_\nu \left(\hat{c}^\dagger_{\nu,j+1}\hat{c}_{\nu,j} + H.c. \right) \right\}. \tag{7}$$

Here, the index $\nu =$ "o" and $\nu =$ "m" refers to the optical and mechanical degrees of freedom. The operators $\hat{c}_{\nu,j}$ denote the annihilation operator for the site j; $\omega_{\nu,j}$ and J_ν denote random on-site frequencies and constant overlap integrals, respectively. The optical and mechanical modes co-localized on the same site are coupled by the radiation pressure force. The resulting interaction reads

$$\hat{H}_{om} = -g_0 \sum_j \hat{c}^\dagger_{o,j}\hat{c}_{o,j}(\hat{c}^\dagger_{m,j} + \hat{c}_{m,j}), \tag{8}$$

where g_0 is the eigenfrequency shift of a localized optical mode by a single phonon on the same site. The presence of a laser drive of frequency ω_L is described by the additional Hamiltonian term

$$\hat{H}_{\rm laser} = \alpha_L \sum_j \hat{c}_{o,j} \exp(i\omega_L t) + H.c. \tag{9}$$

The dynamics of the OMA with the Hamiltonian $\hat{H} = \hat{H}_o + \hat{H}_m + \hat{H}_{\rm om} + \hat{H}_{\rm laser}$ is most conveniently described in the rotating frame defined by the unitary transformation

$$\hat{H} \to \hat{U}\hat{H}\hat{U}^\dagger - i\,\hat{U}\frac{d}{dt}\hat{U}^\dagger, \quad \hat{U} = \sum_j \exp\left(i\omega_L t\, \hat{c}^\dagger_{0,j}\hat{c}_{0,j} \right). \tag{10}$$

We decompose the operators $\hat{c}_{\nu,j}$ as sums of their mean filed values and new displaced operators, $\delta\hat{c}_{\nu,j}$, incorporating the fluctuations, $\hat{c}_{\nu,j} = \langle \hat{c}_{\nu,j} \rangle + \delta\hat{c}_{\nu,j}$. After inserting this decomposition into $\hat{H}$, all linear terms in $\delta\hat{c}_{\nu,j}$ cancel out in the Hamiltonian. We, thus, reproduce Eq.(7) but with the fluctuation operators $\delta\hat{c}_{\nu,j}$ and the detunings $\tilde{\omega}_{o,j} - \omega_L$ replacing the bare operators $\hat{c}_{\nu,j}$ and the optical frequencies $\omega_{o,j}$, respectively. The eigenfrequencies $\tilde{\omega}_{o,j}$ of the optical localized modes include a small power-dependent frequency shift due to a static displacement $\propto 2\mathrm{Re}[\langle \hat{c}_{m,j} \rangle]$ of the corresponding mechanical oscillators, $\tilde{\omega}_{o,j} = \omega_{o,j} - 2g_0\mathrm{Re}[\langle \hat{c}_{m,j} \rangle]$. In the limit where the fluctuations $\delta\hat{c}_{\nu,j}$ are small compared to the mean values (for a strong enough drive), we can neglect all cubic terms and arrive to the linearized opto-mechanical interaction [1]

$$\hat{H}^{(\mathrm{L})}_{\rm om} = -\sum_j \left(g^*_j \delta\hat{c}_{o,j} + H.c. \right) \left(\delta\hat{c}_{m,j} + H.c. \right). \tag{11}$$

Here $g_j \equiv g_0 \langle \hat{c}_{o,j} \rangle$ are the couplings of the linearized interaction. In the main text, we have investigated a parameter regime where the laser is red-detuned compared to all optical resonances. We have also focused on the OMAs where the broadening of the resonances (set by the typical decay rate κ_o) is smaller than the minimal detuning. In this case, all g_j are real valued, consequently, the time-reversal symmetry is preserved by the OM interaction. Summing all contributions, we obtain the Hamiltonian $\hat{H}$ of the main text. There, for brevity, we use $\hat{c}_{\nu,j}$ and $\omega_{o,j}$ for the fluctuation operators and the detunings, respectively. We follow this convention also below. In the main text, we have also assumed that all linearized couplings g_j are approximately equal, $g_j \approx g$. This approximation holds when the mean value of the onsite detuning is much larger than its typical fluctuations, the optical hopping rate, and the typical optical decay rate. Below, we go beyond this approach investigating fluctuating coupling constants g_j.

2. Calculation of the localization length

2.1 Input/Output formalism

Let us express the elastic part of the photon-photon transmission $T_{oo}(k, j; \Omega)$ in terms of the retarded (photon-photon) Green's function.

The response of the OMA to an additional probe field is described by the standard Langevin equations [S1]:

$$\dot{\hat{c}}_{\nu,j} = i[\hat{H}, \hat{c}_{\nu,j}] - \kappa_{\nu,j}\hat{c}_{\nu,j}/2 + \sqrt{\kappa_{\nu,j}}\hat{c}^{\rm in}_{\nu,j}; \tag{12}$$

where $\hat{c}^{\rm in}_{\nu,j}$ is the input (probe) field. The corresponding output field $\hat{c}^{\rm out}_{\nu,j}$ is given by the input/output relations

$$\hat{c}^{\rm out}_{\nu,j} = \hat{c}^{\rm in}_{\nu,j} - \sqrt{\kappa_{\nu,j}}\hat{c}_{\nu,j}. \tag{13}$$

For a probe laser of frequency $\omega_L + \Omega$ (corresponding to the frequency Ω in the rotating frame) applied at site k we have

$$\overline{\hat{c}^{\rm in}_{o,l}} = \delta_{l,k}\alpha_p e^{-i\Omega t}, \quad \overline{\hat{c}^{\rm in}_{m,l}} = 0, \tag{14}$$

where α_p is the amplitude of the probe laser.

The transmission is defined with the help of the ratio

$$\overline{\hat{c}^{\rm out}_{o,j}} \Big/ \overline{\hat{c}^{\rm in}_{o,k}} = \delta_{j,k} - \sqrt{\kappa_{o,j}}\ \overline{\hat{c}_{o,j}} \Big/ \overline{\hat{c}^{\rm in}_{o,k}}. \tag{15}$$

The Hamiltonian has been linearized, hence, the response of $\overline{\hat{c}_{o,j}}$ to the input field in Eq. (12) is linear. Moreover, for the purpose of calculating $\overline{\hat{c}_{o,j}}$, we can replace the operators $\hat{c}^{\rm in}_{\nu,j}$ in the source terms of the Langevin equation (12) with their mean values $\overline{\hat{c}^{\rm in}_{\nu,j}}$. We can even formally replace all the input terms with the coherent interaction

$$H_I = i\sqrt{\kappa_{o,k}}\left(\hat{c}^\dagger_{o,k}\alpha_p \exp[-i\Omega t] - \hat{c}_{o,k}\alpha_p^* \exp[i\Omega t]\right). \tag{16}$$

Thus, $\overline{\hat{c}_{o,j}}$ is given by the Kubo formula where H_I plays the role of the perturbation. We note that the optomechanical coupling does not conserve the number of excitations and, therefore, $\overline{\hat{c}_{o,j}}$ has both an elastic (frequency Ω in the rotating frame or $\Omega + \omega_L$ in the laboratory frame) and an inelastic (frequency $-\Omega$ in the rotating frame or $-\Omega + \omega_L$ in the laboratory frame) components. The elastic part of transmission is obtained after time averaging:

$$T_{oo}(j,k;\Omega) = \left| \frac{\Omega}{2\pi} \int_0^{\frac{2\pi}{\Omega}} \frac{\overline{\hat{c}^{\rm out}_{o,j}}(t)}{\overline{\hat{c}^{\rm in}_{o,k}}(t)} {\rm d}t \right|^2. \tag{17}$$

Using Eqs.(15–16) and the Kubo formula, we find

$$T_{oo}(j,k;\Omega) = \left|\delta_{j,k} - i\sqrt{\kappa_{o,j}\kappa_{o,k}}\, G^R_{oo}(j,k;\Omega)\right|^2; \quad G_{oo}(j,k;\Omega) = -i\int_0^\infty {\rm d}t\, e^{i\Omega t}\, \overline{[\hat{c}_{o,j}(t), \hat{c}^\dagger_{o,k}(0)]}. \tag{18}$$

For $j \neq k$, we recover the formula for $T_{oo}(j,k;\Omega)$ given in the main text.

If the eigenstates of the OMA are localized then $T_{oo}(j,k;\Omega)$ decays exponentially on large distances and the inverse localization length can defined as follows:

$$\frac{1}{\xi(\Omega)} = -\lim_{x\to\infty} \frac{\ln\left[T_{oo}(j,k;\Omega)\right]}{2x} = -\lim_{x\to\infty} \frac{\ln|G^R_{oo}(j,k;\Omega)|}{x}; \quad x \equiv |j-k|. \tag{19}$$

We note that Eq.(19) contains only matrix elements of the Green's function relating operators from sites j and k. These elements can be calculated iteratively with the help of the Dyson's equation which is similar to that suggested in Ref.[S2] for the transfer matrix (details of the algorithm can be found in Ref.[S3]).

Generically, one can introduce 4 transmissions in the elastic channel, $T_{\nu\nu'}(j,k;\Omega)$, and 4 transmissions in the inelastic one, $\tilde{T}_{\nu\nu'}(j,k;\Omega)$ (e.g., the photon-photon transmission, inelastic photon-photon transmission). Similar to Eq.(18), these transmissions are described by entries of the matrix Green's function constructed from four-component "Opto-mechanical×Nambu"-spinors $\hat{C}_j$:

$$\hat{C}^{\rm T}_j(t) = \left\{\hat{c}_{o,j}(t), \hat{c}_{m,j}(t), \hat{c}^\dagger_{o,j}(t), \hat{c}^\dagger_{m,j}(t)\right\}; \tag{20}$$

$$\hat{\mathcal{G}}^R(j,t;j',t') = {\rm i}\theta(t-t')\overline{\hat{C}_j(t)\otimes\hat{C}^\dagger_{j'}(t') - \hat{C}^*_{j'}(t')\otimes\hat{C}^T_j(t)}. \tag{21}$$

$\hat{\mathcal{G}}^R$ has 16 entries which can be obtained from a straightforward generalization of the Dyson equation for the matrix Green's function in frequency space, $\hat{\mathcal{G}}^R(j,j';\Omega)$. We have solved the generalized Dyson equation numerically for the

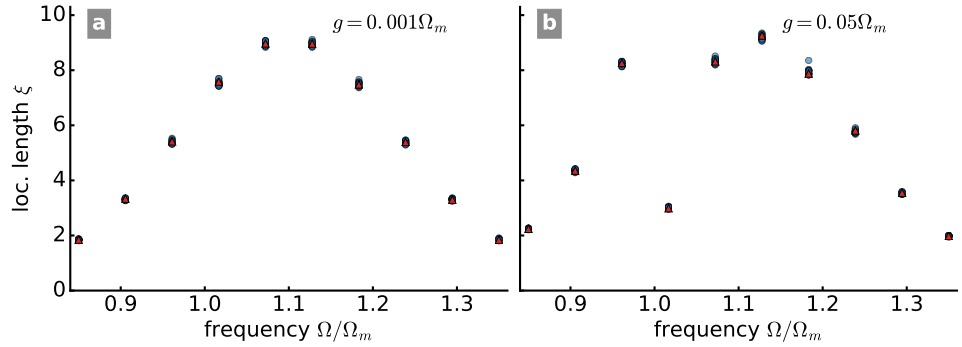

FIG. 5. Blue dots: 16 localization lengths obtained after inserting each entry of $\hat{\mathcal{G}}^R$ into Eq.(19). Red dots are obtained from Eq.(23). Ten different values of the frequency have been taken to demonstrate that all components of the matrix Green's function show the same spatial decay. Parameters of the OMA are the same as in the main text: $\Omega_o = 1.1\Omega_m, J_o = \sigma_o = 0.1\Omega_m, J_m = \sigma_m = 0.001\Omega_m$, $g = 0.001\Omega_m$ (left panel) and $g = 0.05\Omega_m$ (right panel). Numerics were done in the absence of dissipation.

parameters of the OMA given in the main text and compared 16 largest localization lengths governed by inserting each component of $\hat{\mathcal{G}}^R$ into Eq.(19). These localization lengths coincide up to small numerical errors $\leq 1\%$, see blue dots in Fig.5. This is the related to the symmetries, namely, particle-antiparticle symmetry, time-reversal symmetry, and space-inversion symmetry. The latter appears effectively in the long disordered OMAs due to the self-averaging. The equivalence of the different transmissions on large distances allows one to find the largest localization lengths of the OMA from any convenient linear combination of $|\hat{\mathcal{G}}^R_{ab}(j,j';\Omega)|$ ensuring a good convergence of the numerical algorithm. In particular, we can use "the generalized transmission" of the opto-mechanical excitations

$$\mathcal{T}(j,k;\Omega) = \mathrm{Tr}\left(|\hat{\mathcal{G}}^R(j,k;\Omega)|^2\right); \tag{22}$$

and, after disorder averaging, arrive at:

$$\frac{1}{\xi_2(\Omega)} = -\lim_{x\to\infty} \frac{\langle \ln\left[\mathcal{T}(j,k;\Omega)\right]\rangle_d}{2x}, \quad x \equiv |j-k|. \tag{23}$$

Eq.(23) has been used in the numerical code with the disorder averaging being substituted by the self-averaging of ξ in very long systems, see red dots in Fig.5.

2.2 Bogoluibov eigenstates

In the absence of dissipation, there is a simple method which allows one to find the localization length directly from the average number of the excitation. This approach is realized after diagonalizing the Hamiltonian (or, equally, the Heisenberg equations of motion) with the help of the Bogoliubov transformation. Let us define eigenmode operators $\hat{d}_s$. Generically, $\hat{d}_s$ can be written as follows:

$$\hat{d}_s = \sum_{j=1}^{N} \sum_{\nu} \left[u^{(\nu)}_{j,s}\, \hat{c}_{\nu,j} + v^{(\nu)}_{j,s}\, \hat{c}^{\dagger}_{\nu,j} \right], \quad 1 \leq s \leq 2N\,. \tag{24}$$

Here $u^{(\nu)}_{j,s}$ and $v^{(\nu)}_{j,s}$ are the Bogoliubov coefficients. The transformation matrix that diagonalize the Heisenberg equations reads as:

$$T = \begin{bmatrix} U^{(o)} & \left[V^{(o)}\right]^* \\ U^{(m)} & \left[V^{(m)}\right]^* \\ V^{(o)} & \left[U^{(o)}\right]^* \\ V^{(m)} & \left[U^{(m)}\right]^* \end{bmatrix}, \tag{25}$$

where $U^{(\nu)}$ and $V^{(\nu)}$ are $N \times 2N$ matrices whose entries are the coefficients $u_{j,s}^{(\nu)}$ and $v_{j,s}^{(\nu)}$ from Eq.(24). In the absence of dissipation and instabilities, these coefficients satisfy the following relation:

$$\sum_{j=1}^{N} \sum_{\nu} \left\{ u_{j,s}^{(\nu)} \left[u_{j,s'}^{(\nu)} \right]^* - v_{j,s}^{(\nu)} \left[v_{j,s'}^{(\nu)} \right]^* \right\} = \delta_{s,s'}. \tag{26}$$

The minus sign in front of summands $v_{j,s}^{(\nu)} \left[v_{j,s'}^{(\nu)} \right]^*$ is caused by the bosonic commutation relations of the operators $\hat{c}_{\nu,j}$. As a consequence, T is pseudounitary with the inverse matrix

$$T^{-1} = \begin{bmatrix} \left[U^{(o)}\right]^\dagger & \left[U^{(m)}\right]^\dagger & -\left[V^{(o)}\right]^\dagger & -\left[V^{(m)}\right]^\dagger \\ -\left[V^{(o)}\right]^{\mathrm{T}} & -\left[V^{(m)}\right]^{\mathrm{T}} & \left[U^{(o)}\right]^{\mathrm{T}} & \left[U^{(m)}\right]^{\mathrm{T}} \end{bmatrix}. \tag{27}$$

The time evolution of the operators $\hat{c}_{\nu,j}$ can be obtained using Eq. (27), and it is given by

$$\hat{c}_{\nu,j}(t) = \sum_{s=1}^{2N} \left\{ \left[u_{j,s}^{(\nu)} \right]^* \hat{d}_s(0) e^{-i\varepsilon_s t} - v_{j,s}^{(\nu)} \hat{d}_s^\dagger(0) e^{i\varepsilon_s t} \right\}. \tag{28}$$

Here ε_s is the frequency of the hybrid (opto-mechanical) eigenmode s. Using Eqs.(28), one can derive

$$\langle 0 | \hat{d}_s \hat{n}_{\nu,j} \hat{d}_s^\dagger | 0 \rangle = \left| u_{j,s}^{(\nu)} \right|^2 + \left| v_{j,s}^{(\nu)} \right|^2 + \sum_s \left| v_{j,s}^{(\nu)} \right|^2; \quad \langle 0 | \hat{n}_{\nu,j} | 0 \rangle = \sum_s \left| v_{j,s}^{(\nu)} \right|^2; \tag{29}$$

and find the total average number of excitations at a given site j after the eigenmode s is excited:

$$n_j(s) = \langle 0 | \hat{d}_s \hat{n}_j \hat{d}_s^\dagger | 0 \rangle - \langle 0 | \hat{n}_j | 0 \rangle = \sum_\nu \left(\left| u_{j,s}^{(\nu)} \right|^2 + \left| v_{j,s}^{(\nu)} \right|^2 \right), \ \hat{n}_j = \hat{n}_{o,j} + \hat{n}_{m,j}. \tag{30}$$

We have subtracted the (background) fluctuations of $\hat{n}_j$ in the ground state since the number of excitation in the OMA always fluctuates due to the optomechanical coupling, see the second term in the RHS of Eq.(1).

The eigenmodes of the OMA can be found via the numerical diagonalization of the Heisenberg equations. Now we substitute $n_j(s)$ for $\mathcal{T}_{oo}(j,k,\Omega)$ in Eq.(5) and associate the frequency Ω with ε_s and the origin k with the coordinate where the eigenmode s has maximal amplitude. This yields the second expression for ξ_2. Thus, the localization length can be estimated from a log-linear fit of $n_j(s)$, see the discussion of Eq.(5) in the main text.

3. Weak coupling regime, $\Delta_{\mathrm{loc}}^{(\mathrm{m})} \le g \le J_m \ll \sqrt{J_m J_o}$

Let us analyze the behavior of $\xi_2(g)$ for the case $g \le J_m \ll \sqrt{J_m J_o}$ where the influence of the optomechanical coupling on the band structure is negligible. The numerical analysis shows that $\xi_2(g)$ is sub-linear, see the left panel of Fig.6, which indicates the presence of non-perturbative contributions. The full theory for this is missing and we give only phenomenological arguments which are similar to those of the Mott theory [S4] and allow one to explain the sub-linear growth of ξ_2 when g increases up to J_m. For simplicity, we concentrate on the transmission $\mathcal{T}_{om}$ in the regime $\Delta_{\mathrm{loc}}^{(\mathrm{m})} \sim J_m/\xi_m^{(0)} \lesssim g \ll J_m$. Other parameters correspond to Fig.3a in the main text.

Finite transmission $\mathcal{T}_{om}$ requires hybridization of bare optical and mechanical states. The main idea of the phenomenological approach is to find a pair of the optical- and the mechanical- states which, being strongly hybridized, provides the largest possible increase of ξ_2. In other words, we have to estimate the maximal distance between bare localization centers which does not violate the necessary condition for the strong hybridization.

Consider an optical state with the frequency inside the unperturbed mechanical band, $\Omega_m - J_m < \epsilon_o < \Omega_m + J_m$, see the blue wave-function in the right panel of Fig.6. The space coordinates will be counted from the localization center of this optical state. Such a state can be strongly hybridized with the mechanical states if inequality

$$g \, \langle M_j | O \rangle \ge |\epsilon_o - \epsilon_{m,j}|, \tag{31}$$

holds true. Here j is the number of the mechanical state with the localization center at $x_j > 0$ and with the frequency $\epsilon_{m,j}$; $\langle M_j | O \rangle$ is the overlap between the localized optical and the localized mechanical states

$$\langle M_j | O \rangle \sim \left[\xi_m^{(0)} \exp\left(-x_j/\xi_m^{(0)} \right) - \xi_o^{(0)} \exp\left(-x_j/\xi_o^{(0)} \right) \right] \Big/ \left(\xi_m^{(0)} - \xi_o^{(0)} \right). \tag{32}$$

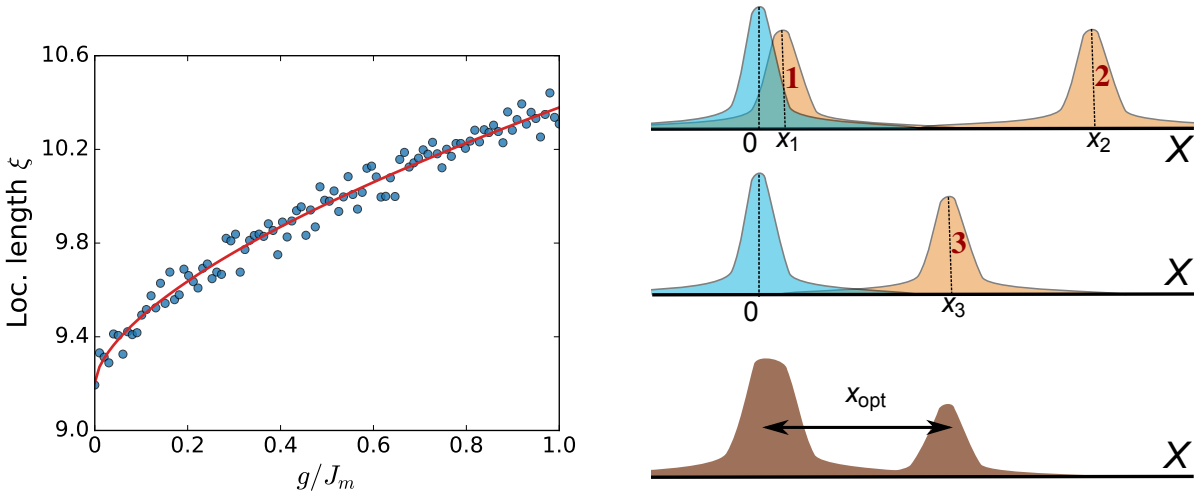

FIG. 6. Left panel: Numerically obtained dependence $\xi_2(g)$ for $g \leq J_m$, $\Omega = \Omega_m$ (shadowed dots). The red line is an example of the fitting which demonstrates the sub-linear nature of this dependence. Right panel: a bare optical state (with blue filling) can be hybridized with different bare mechanical states (with orange filling). The hybridization with the state No.1 is strong but it is unable to change the largest localization length substantially. The hybridization with the state No.2 is negligible. The hybridization with the (optimal) state No.3 is also strong and is responsible for the increase of ξ_2. The optical state being hybridized with the mechanical states No.1,3 yields a "double-hump" optomechanical state (with brown filling) which is responsible for the transmission $\mathcal{T}_{om}$ on large distances.

We recall that $\xi_m^{(0)} > \xi_o^{(0)}$ for $\Omega \simeq \epsilon_o$, cf. Fig.3a.

Firstly we note, that, unlike the Mott theory, frequencies ϵ_o and $\epsilon_{m,j}$ are not correlated at $g = 0$. Therefore, $|\epsilon_o - \epsilon_{m,j}|$ can be arbitrary small even if the localization centers of the bare states are close to each other, $x_j \ll \xi_{o,m}^{(0)} \Rightarrow \langle M_j|O\rangle \sim 1$, see the orange state No.1 in the right panel of Fig.6. On the other hand, it is clear that the 1st mechanical state is unable to support an essential increase of the transmission $\mathcal{T}_{om}$ beyond the bare localization length.

$\mathcal{T}_{om}$ can become more long-ranged if $\xi_m^{(0)} \lesssim x_j$. In the extreme case $\xi_o^{(0)} \ll \xi_m^{(0)} \ll x_j$, the overlap becomes exponentially small, $\langle M_j|O\rangle \sim \exp(-x_j/\xi_m^{(0)})$. Distant mechanical states do not obey the condition Eq.(31) and, therefore, are unimportant, cf. the orange state No.2 in the right panel of Fig.6. However, there is always an optimal state for which x_j is relatively large and the smallness of $\langle M_j|O\rangle$ in Eq.(31) is compensated by the smallness of the frequency separation:

$$\text{optimal state:} \quad \langle M_j|O\rangle \sim \frac{|\epsilon_o - \epsilon_{m,j}|}{g} \;\Rightarrow\; x_{\rm opt} \sim \xi_m^{(0)} \log\left(g \Big/ \Delta_{\rm loc}^{(\rm m)}\right); \tag{33}$$

cf. the orange state No.3 in the right panel of Fig.6. Now we can speculate that, if $\Delta_{\rm loc}^{(\rm m)} \sim J_m/\xi_m^{(0)} \lesssim g \ll J_m$, $\mathcal{T}_{om}$ on large distances and, correspondingly, ξ_2 are governed by the "double-hump" optomechanical state originating mainly from hybridization of the optical state with the optimal mechanical one, see an example in the right panel of Fig.6. Therefore, the largest localization length can be estimated as

$$\xi_2 \simeq \xi_m^{(0)} + \text{const} \times x_{\rm opt} \simeq \xi_m^{(0)} \left[C_1 + C_2 \log\left(g \Big/ \Delta_{\rm loc}^{(\rm m)}\right)\right]. \tag{34}$$

($C_{1,2}$ are constants of order $O(1)$ which cannot be determined in the frame of the phenomenological approach). The optomechnical state may be "multiple-hump" if x_3 covers several localization volumes of the bare mechanical states. If $g \ll \Delta_{\rm loc}^{(\rm m)}$ we expect a crossover to the purely perturbative regime.

Since $\Delta_{\rm loc}^{(\rm o)} \gg J_m \sim \sigma_m$, the minimal space distance between two optical states belonging to the frequency range of the mechanical band is large. We estimate it as $\xi_o^{(0)}\Delta_{\rm loc}^{(\rm o)}/J_m \gg x_{\rm opt}$. This condition allows us to consider relevant optical states independently.

The universal dependence Eq.(34) can be justified only if the frequency range from $\Delta_{\rm loc}^{(m)}$ to J_m is broad and $x_{\rm opt} \gg \xi_m^{(0)}$. This is not the case for the parameters of the main text, in particular, because the disorder is strong.

The fitting in the left panel of Fig.6 can be done equally by using either Eq.(34) or a power-law dependence with some non-universal exponent $\alpha < 1$. More rigorous theory of the weak coupling regime can be developed by exploiting basic ideas of the virial expansion, see Refs.[55] and [S5,S6] for more details.

4. Localization of hybrid excitations in the case of fluctuating coupling constant

In the main text, we have concentrated on the case where the optomechanical coupling g is one and the same for all cells. In reality, the coupling fluctuates: g_j depends on the mean occupation number of the photons on the site j, $g_j \propto c_{o,j}$, while the cells with smaller optical frequencies host more photons, see Fig.7. This locally enhances g_j on these sites. One can speculate that the coupling constant acquires an effective frequency dependence; g becomes larger for smaller frequencies and it slightly decreases with increasing the frequency. We note that $\alpha(\omega_{0,j})$ depicted in Fig.7 is defined as $\alpha(\omega_{0,j}) = c_{o,j}|_{g_0=0}$. We do not distinguish $\alpha(\omega_{0,j})$ and $c_{o,j}$ since their difference is small, $(\alpha(\omega_{0,j}) - c_{o,j}) \sim O(g_0^2)$.

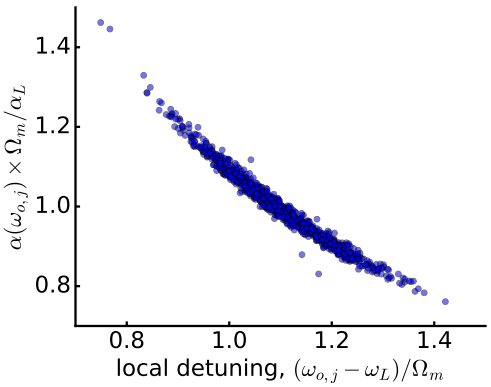

FIG. 7. Dependence of $\alpha(\omega_{0,j}) = c_{o,j}|_{g_0=0}$ on the optical frequency of the cells.

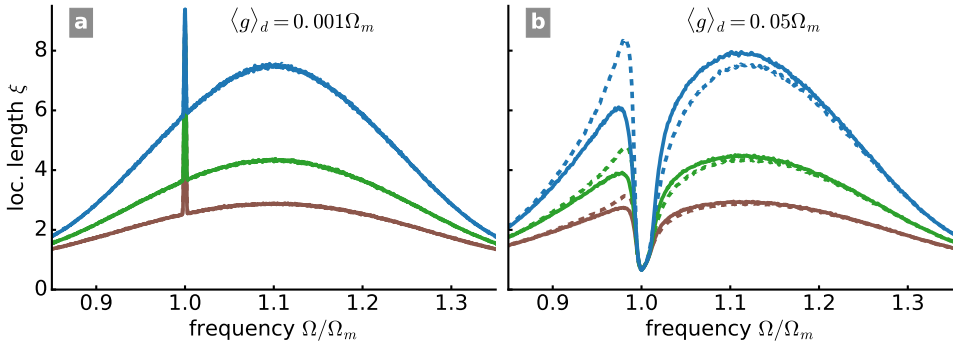

FIG. 8. Frequency dependence of the localization length at $\Omega_o = 1.1\Omega_m$ and $\langle g \rangle_d = g = \{0.001, 0.05\}\Omega_m$ calculated for different values of the optical decay rate $\kappa_o/\Omega_m = \{0.01, 0.05, 0.1\}$ (blue-, green-, and brown lines, respectively). Solid/dashed lines show profiles with/without fluctuations of the coupling constant.

We have recalculated curves from Fig.4 for fluctuating g_j. Results are shown in Fig.8. The disorder averaged coupling has been adjusted to the same values (a) $\langle g \rangle_d = g = 0.001\Omega_m$; and (b) $\langle g \rangle_d = g = 0.05\Omega_m$. Solid/dashed lines show the frequency dependence of the localization length with/without fluctuations of the coupling. The profiles at smaller g are almost intact by its fluctuations. When the mean coupling is larger, the left (right) maximum of $\xi_2(\Omega)$ is suppressed (enhanced) by these fluctuations. This can be explained if, based on Fig.7, we assume that g becomes effectively larger (smaller) at $\Omega < \Omega$ ($\Omega > \Omega$) and notice that the peaks decrease when g increases, cf. Fig.3. Thus, the fluctuations of g_j are able to modify the shape of $\xi_2(\Omega)$ at relatively large values of the mean coupling constant g though all qualitatively important features are expected to be robust.

[S1] C. C. Gerry, P. L. Knight, *Introductory quantum optics*, Cambridge Univ. Press (2005).

[S2] A. MacKinnon and B. Kramer, Phys. Rev. Lett. **47**, p.1546 (1981).

[S3] A. MacKinnon and B. Kramer, Zeitschrift für Physik B Condensed Matter **53**, pp.1-13 (1983).

[S4] N. F. Mott, Philosophical Magazine **22** pp.7-29 (1970).

[S5] O. Yevtushenko, and A. Ossipov, J. Phys. A: Math. Theor. **40**, pp.4691-4716 (2007).

[S6] S. Kronmüller, O.M. Yevtushenko, and E. Cuevas, J. Phys. A: Math. Theor. **43**, 075001 (2010).